Freezing the Nonclassical Crystal Growth of a Coordination Polymer Using Controlled Dynamic Gradients

Marta Rubio-Martinez, Inhar Imaz, Neus Domingo, Afshin Abrishamkar, Tiago Sotto Mayor, René M. Rossi, Carlos Carbonell, Andrew J. deMello, David B. Amabilino, Daniel Maspoch, and Josep Puigmartí-Luis**

Manually engineered self-assembled structures have for many years been investigated under equilibrium conditions so that their most stable forms are reached,[1–5] until recently. There has been a growing interest in obtaining and studying nonequilibrium self-assembled structures.[6–9] The primary reason for this is that nonequilibrium structures (which are typically formed transiently under a constant influx of energy)[10] can offer a broad number of intriguing opportunities in the development of novel materials and systems with advanced functionalities.[11] For example, transient and/or steady-state self-assembled structures generated far from equilibrium are the basis of many sophisticated functions observed in living systems, e.g., DNA replication and/or cell division.[10] Nonetheless, the controlled synthesis and study of intermediate, self-assembled structures is still a major challenge, which currently limits advancements in materials development and technology.

Dr. M. Rubio-Martinez, Dr. I. Imaz, Dr. N. Domingo, Dr. C. Carbonell
Catalan Institute of Nanoscience and Nanotechnology (ICN2)
CSIC and The Barcelona Institute of Science and Technology
Campus UAB, Bellaterra
08193 Barcelona, Spain

A. Abrishamkar, Dr. T. S. Mayor, Dr. R. M. Rossi
Dr. J. Puigmarti-Luis
Empa
Swiss Federal Laboratories for Materials Science and Technology
Lerchenfeldstrasse 5, CH-9014 St. Gallen, Switzerland
E-mail: josep.puigmarti@empa.ch

A. Abrishamkar, Prof. A. J. deMello
Institute of Chemical and Bioengineering
Department of Chemistry and Applied Biosciences
ETH Zurich
Vladimir-Prelog-Weg 1, CH-8093 Zurich, Switzerland

Prof. D. B. Amabilino
School of Chemistry
The University of Nottingham
University Park, NG7 2RD, UK

Prof. D. Maspoch
Catalan Institute of Nanoscience and Nanotechnology (ICN2)
CSIC and The Barcelona Institute of Science and Technology
Campus UAB, Bellaterra, 08193 Barcelona, Spain
E-mail: daniel.maspoch@icn2.cat

Prof. D. Maspoch
Institució Catalana de Recerca i Estudis Avançats (ICREA)
Pg. Lluis Companys 23, 08010 Barcelona, Spain

DOI: 10.1002/adma.201506462

Crystals are an important type of self-assembled structures, where both long range order and control at the molecular level are central characteristics.[12,13] In contrast to living systems, where energy dissipating processes allow the appearance of adaptive and emergent functionalities, crystalline ensembles are frequently studied in their thermodynamically stable forms, where final structures are ultimately determined by chemical equilibria, diffusion, and mass transport processes.[14] Even though crystals, once formed, are static structures that can be investigated at the atomic scale, it has proved difficult to establish methods that can precisely "uncover" their self-assembly process into the most thermodynamic stable forms.[15,16] The most frequent approach employed to understand and control the self-organization of crystalline matter involves varying the functional groups incorporated within their constituent units.[17] This heuristic approach (based on crystal engineering) has proved to be efficient in controlling the self-assembly of molecular components into intricate functional structures.[18] While there is a tremendous interest in rationalizing the crystallization process through the modification of the functional groups present in the molecular building blocks, there is a recognized dearth of methods and processes which allow the isolation and study of out-of-equilibrium species. In this respect, it is important to note that nonequilibrium crystal forms are not only useful in "uncovering" the self-assembly process of crystalline matter, but valuable in rationalizing new artificial materials and systems with advanced functionalities.

As crystallization is inherently a kinetic self-assembly process,[15,19–21] dynamic processing technologies such as microfluidics – where molecules can react under diffusion-controlled conditions[22–24] – can be used to control and investigate out-of-equilibrium processes. For example, controlled reaction–diffusion systems (such as those encountered in hydrodynamic flow focusing mixers)[25] can be utilized in this respect due to the precise spatial and temporal control over concentration profiles and mass transport.[26,27] That is, under hydrodynamic flow focusing conditions, the average residence time and the width of the reaction zone formed between two-reagent streams (where the diffusive mixing occurs) can be precisely controlled.[28,29] Herein, we show for the first time that reaction and/or diffusion-limited (microfluidic) environments can induce concentration gradients that facilitate the formation of novel and exceptionally ordered out-of-equilibrium structures during the crystallization of a coordination polymer (CP). In contrast to macroscopic reaction environments, we prove (both experimentally and through numerical simulations) that dynamic microfluidic conditions allow the isolation

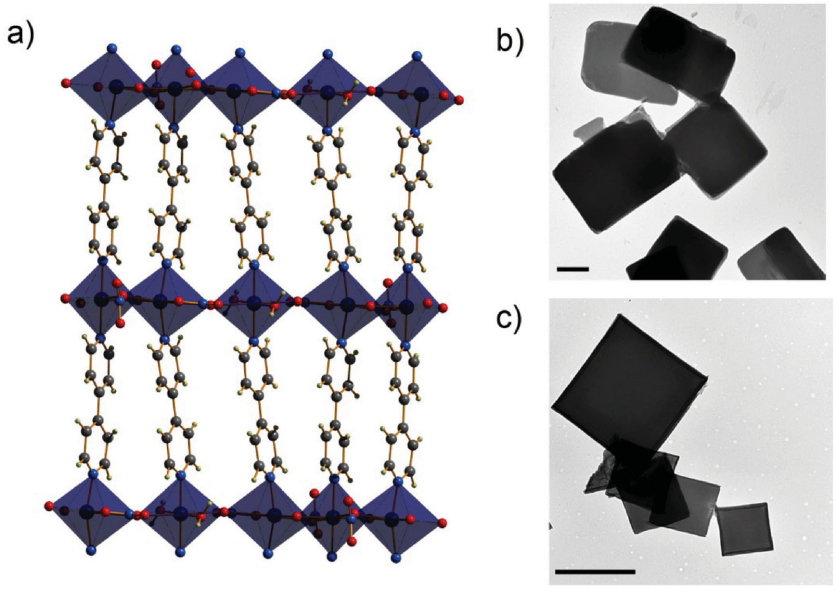

Figure 1. Coordination polymer structure. a) Crystal structure of **1**. b,c) representative TEM images showing the plate-like crystals synthesized through b) conventional mixing of reactants and c) under microfluidic conditions with an FRR of 0.1. Scale bars are 2 μm.

of out-of-equilibrium crystal states through the fine-tuning of reaction times and reagent concentration profiles. We focus our studies on the crystallization process of a CP because of the broad number of applications that these materials have brought onto the scene of crystalline matter.[30,31]

From the vast number of CPs that could be employed in our investigations, we demonstrate the above concept by adopting a 2D CP having the formula $[Cu(4,4'\text{-bpy})](NO_3)_2$ (hereafter **1**; where 4,4′-bpy is 4,4′-bipyridine), which is constructed by connecting μ_2-oxo-bridged and μ_2-NO_3-bridged Cu(II) chains through 4,4′-bpy linkers (**Figure 1**a, Table S1 and Figure S1, Supporting Information). **1** is particularly well-suited to the current investigation since it is easily crystallized (by diffusion of an ethanolic solution of 4,4′-bpy into an aqueous solution of $Cu(NO_3)_2\cdot 6H_2O$ or by mixing the two solutions with or without stirring), and crystallizes in the form of plate-like crystals (Figure 1b); a common crystal habit and one whose self-assembly and crystal growth development are unexplored.[32]

Figure 2a shows the planar microfluidic device employed in the current investigations. This comprises four input channels and one outlet channel (see the Experimental Section for further details). Two inlet channels are used to inject a pair of sheath flows (Q_1 and Q_4) with the two other channels being used to supply the reagent solutions; one containing $Cu(NO_3)_2\cdot 6H_2O$ (Q_2) and the other containing 4,4′-bpy linker (Q_3). The microfluidic device was fabricated in polydimethylsiloxane (PDMS) using standard soft-lithographic methods and was covered by a glass cover slide (see Experimental Section for further details). We defined the four input channels and corresponding flow rates (in μL per min) as: [flow (1): Q_1, flow (2): Q_2, flow (3): Q_3, flow 4: Q_4]. Reactions were formed by hydrodynamically injecting water (Q_1), a 100×10^{-3} M aqueous solution of $Cu(NO_3)_2\cdot 6H_2O$ (Q_2), a 100×10^{-3} M ethanolic solution of 4,4′-bpy (Q_3), and an ethanol flow (Q_4). The reactant concentrations were optimized to guarantee rapid crystallization whilst ensuring that microfluidic channels do not block. In initial studies, we investigated the crystallization of **1** by varying the flow-rate ratio (FRR), whilst keeping the reagent flow rates (Q_2 and Q_3) constant. The FRR is defined as the ratio of flow between the focusing streams and the reagent fluids (i.e., $FRR = (Q_1+Q_4)/(Q_2+Q_3)$). In all cases, crystals of **1** were immediately formed at the interface between the Cu(II) ion and 4,4′-bpy streams after injection. The resulting crystals were collected on transmission electron microscopy grids, filter paper and/or diluted on ethanol at the end of the main channel to avoid off-chip reactions. Subsequently, the crystals formed were further characterized by field-emission scanning electron microscopy (FE-SEM), transmission electron microscopy (TEM), polarising optical microscopy (POM), and X-ray powder diffraction (XRPD).

Figures 1c, 2c (right), and **3**b (right) show typical TEM and FE-SEM images of crystals of **1** prepared at FRR of 0.1. These crystals that have a square plate-like habit are representative of those synthesized either by conventional diffusion or simple mixing in a macroscopic vessel (Figure 1b). This is expected since as the FRR decreases at a constant overall flow rate, the width of the diffusive mixing zone at the interface between the two reagent streams increases as a function of distance along the channel (i.e., a nonsharp concentration gradient is generated). Accordingly, the reaction zone in which the structures assemble is enlarged, thus mimics to some extent conventional diffusion on the macroscale, and assembly of the most thermodynamic stable structures will be favored. Finite element simulations strongly support the idea that a decrease in the FRR prompts an increase in the reaction–diffusion zone present along the length of the main microfluidic channel where crystallization takes place (Figure S2, Supporting Information). Crystals of **1** prepared at an FRR of 0.1 had average dimensions of 2.80 ± 0.52 μm. In addition, both the simulated (derived from the single crystal structure of **1**) and experimental (resulting from the crystals synthesized at an FRR of 0.1) XRPD patterns are consistent (Figure 2b; Figure S3, Supporting Information), confirming that crystals synthesized in the microfluidic system are structurally identical to crystals prepared through conventional methods. Additionally, it is noted that **1** can be obtained as phase pure; even though the precipitation of a small amount of free 4,4′-bpy ligand is detected.

As shown in Figure 2c, we then varied the FRR from 0.1 to 5 and observed the formation of numerous and unprecedented nonequilibrium crystal morphologies. In contrast to previous studies, where blocking agents are used to study intermediate states during a crystal growth process,[33] in the current investigations the ultimate shape of all generated structures solely depends upon the conditions established within the diffusive mixing zone. Increasing the FRR whilst keeping the reagent flow rates constant, a rationalized reduction of the diffusive mixing zone can be achieved (i.e., a sharp concentration

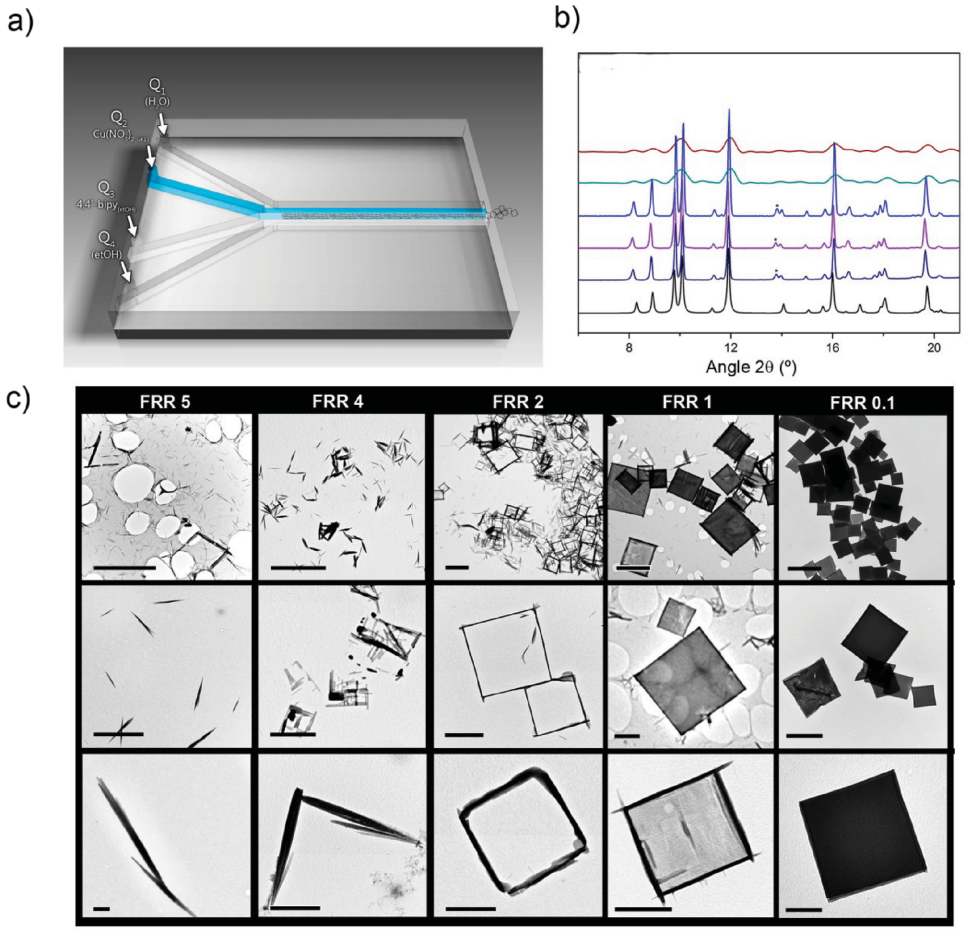

Figure 2. Morphological transitions of coordination polymer 1 using microfluidics. a) Schematic illustration of the microfluidic device and the configuration of both reactant and sheath flows. b) XRPD patterns of 1: simulated (black), synthesized at an FRR of 0.1 (dark blue), 1 (violet), 2 (blue), 4 (green), and 5 (red). Peaks marked with asterisks correspond to the precipitation of the free 4,4′-bpy ligand. c) Sequence of TEM images of crystals of 1 fabricated in the microfluidic device at different FRRs with three different magnification levels, showing trapped crystalline phases that range from needles to hollow frames to plate-like crystals (left to right). Scale bars: 5 μm (top row), 2 μm (middle row), and 1 μm (bottom row).

gradient is generated, see Figure S2, Supporting Information), which leads to diffusion-limited and kinetically controlled environments in which the formation of the most thermodynamic stable crystal forms can be avoided to some extent.[34,35] That is, at high FRR crystals form at high supersaturation conditions; a result that promotes the formation of out-of-equilibrium crystal forms.[36] For example, we observed the formation of needles at an FRR of 5; needles that start to orthogonally connect through their edges at an FRR of 4; hollow frames at an FRR of 2; frames partially filled with a thinner layer at FRR of 1; and the above-mentioned square plate-like filled crystals at FRR of 0.1. Importantly, varying the total flow-rate (TFR) without varying the FRR provides a direct way of controlling the average residence (reaction) time for crystallization and thus throughput, but has no significant effect on the habits and structures generated (Figure S4, Supporting Information). Here, only slight differences on the crystal size were observed. To further understand these experimental results, numerical simulations were performed. Finite element data show that the overall concentration profiles of the reagents do not change drastically when modifying the TFR for a given FRR, but do change remarkably when varying the FRR for a given TFR. In this case, the overall concentration profiles of the reagents become narrower and the maximum concentration is reduced with increasing FRR (Figure S5, Supporting Information). This observation implies that the concentration of reagents present within the microfluidic channel (and which are consumed during the formation of crystals) is reduced at higher FRRs for all TFRs considered, and thus provides for precise control of crystallization kinetics and crystal growth.

The isolated needles obtained when performing crystallization at FRR of 5 had an average length of 500 nm and a diameter of 20 nm. At a lower FRR of 4, we detected the coexistence of identical needles with some structures comprising two or three needles perpendicularly connected at their edges. Interestingly, at FRR of 2, hollow frames, with average side dimensions of 2.95 ± 0.71 μm and edge thicknesses of 200 nm, were found to be predominant. Further decreasing the FRR to 1 resulted in a partial filling of these hollow frames, finally forming the previously described plate-like crystals seen when a FRR of 0.1 was used.

Moreover, in contrast to other mechanistic studies where amorphous intermediate states of CPs are simply investigated

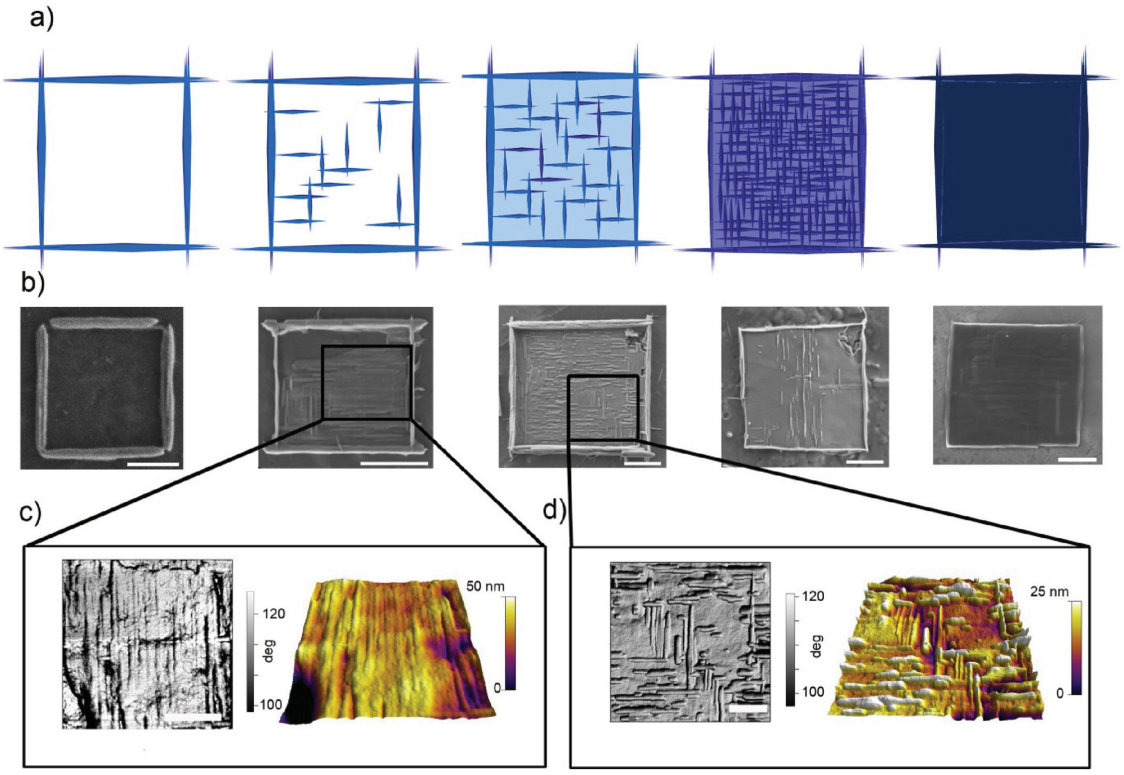

Figure 3. Evolution of crystal growth. a) Schematic representation of the crystal growth of **1** illustrating the progressive filling of the internal area of hollow frames. b) FE-SEM images showing the crystal transformation from hollow frames to plate-like crystals. c,d) AFM images showing the crystal growth of the internal area of the frames at c) initial and d) progressive filling stages. The left hand side images report phase contrast, and right hand side images are 3D graphics of topography. Scale bars: 1 μm

by time-lapse scanning electron microscopy (SEM) imaging analysis,[37–40] in the current investigation all structures generated are crystalline. Accordingly, XRPD studies can provide valuable insights in better understanding and characterizing nanoscale self-organization of the building blocks in their isolated, nonequilibrium forms. XRPD studies were essential to confirm that all crystals generated under diffusion-limited and kinetically controlled microfluidic environments corresponded to **1**. Indeed, as shown in Figure 2b, the XRPD patterns of all crystals obtained at different FRRs perfectly matched that simulated from the crystal structure of **1**. It should be noted that XRPD patterns of the needles obtained at FRRs of 5 and 4 show broad peaks, which are attributed to their lower crystallinity.

To shed light on the growth mechanism that transforms the hollow frames (FRR = 2) to plate-like crystals (FRR = 0.1) (Figure 3a,b), we further analyzed various nonequilibrium crystal forms of **1** using atomic force microscopy (AFM) and POM. In the early stages of frame formation, we were able to confirm that the frames are completely hollow, with no evidence of residues inside the frames (Figure S6, Supporting Information). At the vertices of the frames, the perpendicular needles do not overlap but instead completely interpenetrate (Figure S7, Supporting Information). Additionally, POM indicates that the optic axis of a crystal is the same in all sides of the frame (Figure S7, Supporting Information). The progressive filling of the internal area of the frames typically occurs by parallel needle growth, as observed in Figure 3c. For higher degrees of filling (Figure 3d), precise observation of the filling fractions shows that needles tend to organize orthogonally in alternative growth levels. Some degree of interweaving occurs in areas where full coverage is yet to be achieved, with the needles at subsequent levels filling the gaps. Finally, at some point, needle coalescence occurs and the surface of the area inside the frames becomes uniform, ultimately forming the plate-like crystals.

The detailed mechanism leading to the formation of these ordered out-of-equilibrium structures remains unclear at the current time, however, the process seems to occur so as to lower and/or eliminate high-energy facets in the generated structures; an idea that has previously been suggested by others in regard to the shape-controlled growth of inorganic crystals.[15] Based on these previous studies with inorganic crystals and consideration of the results presented herein, we propose a dynamic crystal growth process as shown in the idealized sequence of Figure 2c. It is likely that needles isolated at a high FFR can act as seeds for the assembly of the nonequilibrium trapped intermediate states, which then evolve toward a final thermodynamic stable form: plate-like crystal structures. This proposal is supported by XRPD studies, which prove that all the structures generated have an identical chemical connectivity. Furthermore, the AFM studies support our hypothesis by confirming that growth of **1** is dynamic and that the agglomeration and progressive filling of nonequilibrium forms can occur due to a parallel growth of needle-based structures. The AFM results

therefore suggest that the early stage isolated seeds organize at a single level and in a perpendicular fashion, leading to the final plate-like crystalline morphologies observed in bulk and at an FFR of 0.1 (Figure 1b,c, respectively).

In summary, we have shown that diffusion-limited and kinetically controlled growth regimes occurring in microfluidic devices can provide valuable insights into crystallization processes. In contrast to other methods where trapping of the structures generated during a polymerization process is achieved by taking aliquots in a controlled solvent-induced precipitation regime,[41] we show, for first time, that hydrodynamic flow-focusing condition provided by the adoption of a continuous-flow microfluidic scheme can be a powerful experimental tool for the generation and isolation of nonequilibrium forms. We believe that the microfluidic-based approach presented here circumvents limitations generally ascribed to the isolation and study of transient forms during crystallization processes. We have demonstrated that microfluidic dynamic processing provides an accessible range of nonequilibrium structures present during crystal growth. These results are exciting since the control and prediction of chemical and physical properties in crystalline matter can only be achieved when methods that can precisely uncover the self-assembly process can be established. The technology presented constitutes a potential route toward a wealth of new and improved materials, where the rationalization of controlled chemical and physical properties may become reality.

Experimental Section

Materials and Methods: The reagents $Cu(NO_3)_2{\bullet}6H_2O$ and 4,4′-bipyridine (4,4′-bpy) were obtained from Sigma-Aldrich Co. High purity EtOH was purchased from Teknokroma. Deionised Milipore Mili-Q water was used in all experiments. SEM images were collected on a scanning electron microscope (ZEISS EI MERLIN FE-SEM) at acceleration voltages of 0.2–30 kV. Aluminium was used as support. TEM images were obtained with a JEOL JEM 1400 electron microscope. X-ray EDX microanalysis was performed using an Oxford Instruments INCA energy SEM system. All measurements were performed at room temperature and at a voltage of 120 kV. XRPD measurements were performed using an X'Pert PRO MPD diffractometer (Panalytical) especially configured for in-plane diffraction.

Microfluidic Device Fabrication: The microfluidic channels employed in this study were structured in PDMS (SYLGARD 184 Silicone Elastomer Kit) using an SU-8 (2015, Microchem) master form fabricated by standard photolithographic techniques. Before attaching the cured and structured PDMS mould to a glass coverslip through plasma activation, inlet holes connecting the microfluidic channels were punched with a Biopsy puncher. The cross-sectional dimensions of the microchannels were 50 μm × 50 μm for the four input microchannels, and 250 μm × 50 μm for the main reactor channel. The total length of the main reactor channel was 9 mm.

Synthesis of 1 via Mixture of Reactants: In a typical experiment, an aqueous solution of $Cu(NO_3)_2{\bullet}6H_2O$ (100×10^{-3} M) was added to an ethanolic solution of 4,4′-bpy (100×10^{-3} M) with or without stirring. After a few seconds, blue crystals of **1** were formed. Anal. (%) Calcd. for $C_{20}H_{18}Cu_2N_6O_8,NO_3,H_2O$; C, 35.45; H, 2.97; N, 14.47. Found: C, 35.67; H, 2.69; N, 14.28.

Synthesis of 1 via Diffusion: In a typical experiment, a solution of 4,4′-bpy (100×10^{-3} M) in ethanol and an aqueous solution of $Cu(NO_3)_2{\bullet}6H_2O$ (100×10^{-3} M) were prepared. The solutions were then transferred to a test tube in a manner that generated a distinct interface between the two layers. After 4 d, dark blue crystals of **1** suitable for single-crystal XRD analysis started to form at the liquid–liquid interface. Anal. (%) Calcd. for $C_{20}H_{18}Cu_2N_6O_8,NO_3,H_2O$; C, 35.45; H, 2.97; N, 14.47. Found: C, 35.11; H, 3.12; N, 14.28.

Synthesis of 1 Using Laminar Flow: The syntheses of different crystal morphologies of **1** were carried out in a planar microfluidic device that consists of four input channels and one outlet channel, imprinted in PDMS and was covered by a glass plate. Reactant solutions were injected via a syringe pump system at given flow rates. The flow rates were defined (all in μL/min) using the following abbreviations: flow (1), Q_1; flow (2), Q_2; flow (3), Q_3; and flow (4), Q_4. In a typical synthetic procedure, crystals of **1** were initially prepared by injecting an aqueous solution of $Cu(NO_3)_2{\bullet}6H_2O$ (100×10^{-3} M) in Q_2 and an ethanolic solution of 4,4′-bpy (100×10^{-3} M) in Q_3. Both were accomplished by an auxiliary flow with the corresponding solvents, Q_1 and Q_4.

X-Ray Crystallography: X-ray single-crystal diffraction data for **1** were collected on the BM16 Spanish line of the ESRF synchrotron in Grenoble ($\lambda = 0.7901$ Å). Data were indexed, integrated, and scaled using HKL2000 software.[1] The H atoms were included in theoretical positions but not refined. The low max value was due to the data collection process, which was performed in the BM16 line with only a phi scan. The structure was solved by direct methods using the program SHELXS-97.[2] Refinement and all further calculations were carried out using SHELXL-97. Empirical absorption corrections were applied in both cases using SCALEPACK.[1]

AFM Measurements: Atomic force microscopy images were taken in amplitude modulation dynamic AFM mode, in pure noncontact conditions with an Asylum MFP3D system, using Pt-coated tips (Nanosensors PPP-EFM) and a resonance frequency around 70 kHz. Images were obtained using a scanning rate of 1 Hz and keeping the amplitude of oscillation constant at about 50 nm. For Kelvin probe force microscopy images, an AC voltage of 1 V amplitude was applied to the tip at a distance of 50 nm to the surface, and the surface potential function difference between the tip and the sample was obtained.

Numerical Simulations: The 2D steady-state fluid flow and mass transport across the microfluidic device was simulated using a Finite Element approach, considering geometries and boundary-conditions as described in the manuscript. Diffusion coefficients of both reagents were assumed to be 10^{-9} m^2 s^{-1}, in line with literature data for ethanol-water mixtures.[3] Density and dynamic viscosity of reagents and sheathed currents were assumed to be those of the corresponding pure solvents, i.e., 103 kg m^{-3} and 8.9×10^{-4} Pa•s for water-based currents and 789 kg m^{-3} and 1.1×10^{-3} Pa•s for ethanol-based currents, respectively.

Supporting Information

Supporting Information is available from the Wiley Online Library or from the author.

Acknowledgements

The authors acknowledge the financial support from MINECO-Spain, under projects MAT2012-30994 and CTQ2011-16009-E, the European Research Council under the European Union's Seventh Framework Programme (FP7/2007-2013)/ERC Grant agreement nº 615954 and from the Swiss National Science Foundation (SNF) through the project nº 200021_160174. The authors thank the Microscopy Service of the UAB. M.R.-M. and C.C. thank the ICN2 for their research fellowship, I.I., N.D., and J.P.-L. thank the MINECO for RyC contracts. ICN2 acknowledges the support of the Spanish MINECO through the Severo Ochoa Centers of Excellence Program, under Grant SEV-2013-0295.

Received: December 30, 2015
Revised: May 24, 2016
Published online: July 12, 2016

[1] G. M. Whitesides, M. Boncheva, *Proc. Natl. Acad. Sci. USA* **2002**, *99*, 4769.
[2] S. S. Babu, S. Prasanthkumar, A. Ajayaghosh, *Angew. Chem. Int. Ed.* **2012**, *51*, 1766.
[3] D. Phlip, *Adv. Mater.* **1996**, *8*, 866.
[4] F. J. M. Hoeben, P. Jonkheijm, E. W. Meijer, A. P. H. J. Schenning, *Chem. Rev.* **2005**, *105*, 1491.
[5] I. C. Reynhout, J. J. L. M. Cornelissen, R. J. M. Nolte, *Acc. Chem. Res.* **2009**, *42*, 681.
[6] J. Boekhoven, J. M. Poolman, C. Maity, F. Li, L. van der Mee, C. B. Minkenberg, E. Mendes, J. H. van Esch, R. Eelkema, *Nat. Chem.* **2013**, *5*, 433.
[7] P. A. Korevaar, S. J. George, A. J. Markvoort, M. M. J. Smulders, P. A. J. Hilbers, A. P. H. J. Schenning, T. F. A. De Greef, E. W. Meijer, *Nature* **2012**, *481*, 492.
[8] B. A. Grzybowski, H. A. Stone, G. M. Whitesides, *Nature* **2000**, *405*, 1033.
[9] S. Mann, *Nat. Mater.* **2009**, *8*, 781.
[10] G. M. Whitesides, B. Grzybowski, *Science* **2002**, *295*, 2418.
[11] J. M. A. Carnall, C. A. Waudby, A. M. Belenguer, M. C. A. Stuart, J. J.-P. Peyralans, S. Otto, *Science* **2010**, *327*, 1502.
[12] J.-M. Lehn, *Angew. Chem. Int. Ed.* **1990**, *29*, 1304.
[13] O. M. Yaghi, M. O'Keeffe, N. W. Ockwig, H. K. Chae, M. Eddaoudi, J. Kim, *Nature* **2003**, *423*, 705.
[14] J. Hulliger, *Angew. Chem. Int. Ed.* **1994**, *33*, 143.
[15] S. Mann, *Angew. Chem. Int. Ed.* **2000**, *39*, 3392.
[16] D. Gebauer, M. Kellermeier, J. D. Gale, L. Bergström, H. Cölfen, *Chem. Soc. Rev.* **2014**, *43*, 2348.
[17] M. D. Hollingsworth, *Science* **2002**, *295*, 2410.
[18] J. Kang, D. Miyajima, T. Mori, Y. Inoue, Y. Itoh, T. Aida, *Science* **2015**, *347*, 646.
[19] S. Mann, *Nature* **1988**, *332*, 119.
[20] Y. Yin, A. P. Alivisatos, *Nature* **2005**, *437*, 664.
[21] E. González, J. Arbiol, V. F. Puntes, *Science* **2011**, *334*, 1377.
[22] J. Atencia, D. J. Beebe, *Nature* **2005**, *437*, 648.
[23] R. F. Ismagilov, A. D. Stroock, P. J. A. Kenis, G. Whitesides, H. A. Stone, *Appl. Phys. Lett.* **2000**, *76*, 2376.
[24] P. J. A. Kenis, R. F. Ismagilov, G. M. Whitesides, *Science* **1999**, *285*, 83.
[25] J. B. Knight, A. Vishwanath, J. P. Brody, R. H. Austin, *Phys. Rev. Lett.* **1998**, *80*, 3863.
[26] E. Amstad, M. Gopinadhan, C. Holtze, C. O. Osuji, M. P. Brenner, F. Spaepen, D. A. Weitz, *Science* **2015**, *349*, 956.
[27] W.-Y. Lin, Y. Wang, S. Wang, H.-R. Tseng, *Nano Today* **2009**, *4*, 470.
[28] J. Puigmartí-Luis, D. Schaffhauser, B. R. Burg, P. S. Dittrich, *Adv. Mater.* **2010**, *22*, 2255.
[29] J. Puigmartí-Luis, M. Rubio-Martínez, U. Hartfelder, I. Imaz, D. Maspoch, P. S. Dittrich, *J. Am. Chem. Soc.* **2011**, *133*, 4216.
[30] S. Kitagawa, R. Kitaura, S. Noro, *Angew. Chem. Int. Ed.* **2004**, *43*, 2334.
[31] C. Janiak, *Dalton Trans.* **2003**, 2781.
[32] T. Rodenas, I. Luz, G. Prieto, B. Seoane, H. Miro, A. Corma, F. Kapteijn, F. X. Llabrés i Xamena, J. Gascon, *Nat. Mater.* **2015**, *14*, 48.
[33] X. Sun, S. Dong, E. Wang, *J. Am. Chem. Soc.* **2005**, *127*, 13102.
[34] M. Numata, T. Kozawa, *Chem. Eur. J.* **2013**, *19*, 12629.
[35] M. Numata, Y. Takigami, M. Takayama, T. Kozawa, N. Hirose, *Chem. Eur. J.* **2012**, *18*, 13008.
[36] V. Bhamidi, S. H. Lee, G. He, P. S. Chow, R. B. H. Tan, C. F. Zukoski, P. J. A. Kenis, *Cryst. Growth Des.* **2015**, *15*, 3299.
[37] M. Oh, C. A. Mirkin, *Nature* **2005**, *438*, 651.
[38] Z. Shen, G. Zhang, H. Zhou, P. Sun, B. Li, D. Ding, T. Chen, *Adv. Mater.* **2008**, *20*, 984.
[39] S. Jung, M. Oh, *Angew. Chem. Int. Ed.* **2008**, *47*, 2049.
[40] Y.-M. Jeon, G. S. Armatas, D. Kim, M. G. Kanatzidis, C. A. Mirkin, *Small* **2009**, *5*, 46.
[41] A. M. Spokoyny, D. Kim, A. Sumrein, C. A. Mirkin, *Chem. Soc. Rev.* **2009**, *38*, 1218.